The Origin and Dispersion Characteristics of the Observed Tropical Summertime Synoptic-Scale Waves over the Western Pacific*

CHI-YUNG TAM AND TIM LI

International Pacific Research Center, School of Ocean and Earth Science and Technology, University of Hawaii at Manoa, Honolulu, Hawaii

(Manuscript received 1 April 2005, in final form 15 September 2005)

ABSTRACT

The origin, initiation, and dispersion behavior of the observed summertime synoptic-scale disturbances in the tropical western Pacific are studied. These westward-propagating disturbances have the strongest growth rate over the region of ~130°–160°E off the equator. The three-dimensional wave activity flux associated with a wave packet in the vicinity of this region is computed. In general, wave activity is directed westward. There is accumulation of activity flux, which gives rise to the amplification of waves. In the low levels, such accumulation can be attributed to the convergence of both the mean flow and the intrinsic group velocity. Diabatic forcing also contributes to the growth of disturbances and is most important in the 500–600-hPa layer. Along the east–west-oriented "storm tracks" of the synoptic-scale disturbances, there are two different dynamical regimes. West of ~150°E, enhanced convection is associated with increased specific humidity at the top of the planetary boundary layer and is in phase with positive low-level vorticity anomalies. To the east of 150°E the vorticity leads the convection by about one-quarter of a wavelength. This phase relationship can be explained by adiabatic dynamics and is related to the positive vertical shear of the mean zonal flow in the latter region.

Near and to the east of the date line where disturbances are initiated in the low levels, the heat flux associated with the synoptic-scale eddies is negative (i.e., $v'T' < 0$) from about 300 to 700 hPa. This implies downward-directed wave activity. In the upper troposphere at the same geographical location, there is southward wave activity from the extratropics penetrating into the Tropics. These findings suggest that summertime synoptic-scale disturbances may originate from extratropical forcing. This hypothesis is supported by a case study. Intrusion of high potential vorticity into the Tropics was seen to be followed by downward development, resulting in low-level disturbances that subsequently moved westward in the western Pacific and grew.

1. Introduction

a. Structure and wave characteristics

Tropical synoptic-scale disturbances have interested meteorologists and synopticians for many decades. Riehl (1945) first referred to the disturbances over the Caribbean as "easterly waves." Summertime synoptic-scale waves are believed to be associated with the formation of tropical cyclones over various ocean basins [see the review section of Wallace (1971)]. A number of observational studies (Wallace and Chang 1969; Chang et al. 1970; Reed and Recker 1971) reveal the following characteristics and circulation structure of the disturbances over the western Pacific. In general they propagate to the west or northwest, and have a wavelength of ~3000 km and a period of 4–6 days. Their associated meridional wind fluctuations are most pronounced in the lower troposphere. Lau and Lau (1990, hereafter referred to as LL90) identified regions in the Tropics with enhanced synoptic-scale activity during boreal summer. Coherent and wavelike propagating disturbances exist in these tropical regions, and there is growth (decay) of the waves over the eastern (western) part of the "storm tracks." Over the western Pacific, the wavelength of disturbances is about 2500 km and the phase speed is 5 m s^{-1}.

* School of Ocean and Earth Science and Technology Contribution Number 6677 and International Pacific Research Center Contribution Number 356.

Corresponding author address: Dr. Chi-Yung Tam, International Pacific Research Center, School of Ocean and Earth Science Technology, 1680 East West Road, POST Bldg., Honolulu, HI 96822.
E-mail: chiyung@hawaii.edu

For mature synoptic-scale disturbances, their vertical circulation structure is characterized by a warm anomaly at intermediate levels (from 500 up to ~200 hPa) sandwiched by cold anomalies above and below (see LL90). The low-level "cold core" along the trough axis has been pointed out by many studies (see, e.g., Chang et al. 1970). Warm perturbations are collocated with rising motion. This is consistent with the large conversion from eddy available potential energy to kinetic energy, the former of which is mainly generated from diabatic heating (Lau and Lau 1992). Interestingly, Nitta (1970) and Reed and Recker (1971) found equatorward heat flux at ~700 hPa associated with the synoptic-scale eddies over the western to central Pacific. It is also known that within the lower to middle troposphere, the vertical structure of the waves (as revealed by the meridional wind or the relative vorticity) evolves from being slightly tilted eastward over the central to eastern Pacific, to having little tilt in the western Pacific (Reed and Recker 1971). Variation of the vertical structure can be ascribed to the different vertical wind shear of the mean zonal flow at different longitudes. This argument is supported by the numerical study of Holton (1971), who examined the effects of vertical wind shear on the circulation response to imposed heating in the Tropics.

b. Wave activity and origin of disturbances

Holland (1995) suggested that the confluent structure of the low-level flow over the western Pacific is effective in trapping the energy of short waves. Westward-moving wave packets approaching the region of confluence from the east could be slowed down and amplify. Sobel and Bretherton (1999, hereafter referred to as SB99) furthered these ideas and proposed the accumulation of wave activity as a mechanism for the initial development of synoptic-scale disturbances in the region. Wave activity estimates based on eddy statistics are found to be convergent over most part of the western Pacific. Strong growth rates could result from such convergence of activity. The modeling work of Kuo et al. (2001) is in general agreement with this picture. Eddies are found to grow in simulations using a confluent background flow. Their numerical integrations with a monsoon-like ambient flow field also show southeastward energy dispersion from vortices, resembling that observed in some cases of tropical cyclones genesis. The importance of such a process in cyclone formation was highlighted by Li et al. (2003), who presented case studies of genesis associated with energy dispersion from preexisting tropical cyclones as well as synoptic-scale disturbances.

So far only a few studies address the question of the origin of synoptic-scale disturbances over the western Pacific. SB99 suggested that mature tropical cyclones might be an important in situ source of wave activity in the region. Other possible activity sources can be those with remote origins, such as short equatorial waves (Holland 1995), easterly waves from the eastern Pacific, or perhaps tropical instability waves (TIWs; Legeckis 1977). Based on the low-level v-wind data, Nitta and Takayabu (1985) found no connection between activity over the western Pacific and that over the eastern Pacific. On the other hand, researchers had noticed that upper-tropospheric cold lows might affect the low-level synoptic-scale circulation over the central to western Pacific (see Wallace 1971). Heta (1991) provided evidence that the initiation of easterly waves near the central Pacific is associated with upper-level cold lows at ~20°N with a distinct northeast–southwest tilt. They were cut off from the upper-level mid-Pacific trough and moved westward together with their corresponding cyclonic anomalies at low levels. These findings bear some similarity with those of Kiladis (1998), who studied the convective activity over the eastern Pacific intertropical convergence zone (ITCZ) forced by Rossby waves from the extratropics during northern winter. Downward dispersion is associated with the upper-level Rossby waves, and convection is induced through changes of the static stability accompanying the intrusion of high potential vorticity (PV) into tropical latitudes. As a result, westward-propagating equatorial waves are also excited. It seems plausible that summertime synoptic-scale disturbances could be induced by extratropical activity through mechanisms similar to those described by Kiladis (1998).

In this study the three-dimensional dispersion characteristics of the synoptic-scale waves over the western Pacific, as well as the implications on the growth and the possible origin of theses waves, are examined. To this end, we use the phase-independent wave-activity flux of Takaya and Nakamura (2001), which is generalized here for an easterly basic state. The main focus is on the region east of about 130°E over the western Pacific with low-level mean easterlies. This is in contrast to the study of LL90, whose domain of analyses for the "western Pacific mode" is located farther west where the strongest variability is found. As will be made clear, our choice is relevant for studying the initiation and growth of disturbances. The rest of this paper is organized as follows. Datasets used in this study are described in section 2. Wave characteristics and the circulation associated with the dominant mode of synoptic-scale variability in our analysis domain are given in section 3. Section 4 is about the three-dimensional wave activity associated with the disturbances and the

potential role of extratropical forcing. A case study of synoptic-scale waves induced by upper-level activity is presented in section 5, followed by discussions and conclusions in section 6.

2. Description of datasets

Daily mean products from the National Centers for Environmental Prediction–National Center for Atmospheric Research (NCEP–NCAR) reanalysis project (Kalnay et al. 1996) for the period of 1979 to 2003 serve as the main dataset for this study. Upper-air variables are used. They are archived on a 2.5° × 2.5° latitude–longitude grid, and on 17 pressure levels. We keep in mind that while the winds, geopotential, and upper-air temperature should be close to observations, other variables such as the vertical velocity could be strongly model dependent (Kistler et al. 2001).

Apart from NCEP–NCAR reanalyses, outgoing longwave radiation (OLR) daily data from the National Oceanic and Atmospheric Administration (NOAA), Quick Scatterometer (QuikSCAT) level 3 surface winds interpolated on a 0.5° × 0.5° grid, and reanalysis products from the European Centre for Medium-Range Weather Forecast (ECMWF) 40-yr Re-analysis Project (ERA-40) are also used in part of this work. Analyses based on these different datasets are reasonably consistent with each other; this gives confidence that our results are not artifacts of the assimilation models.

3. Western Pacific synoptic-scale activity

During boreal summer, synoptic-scale activity with well-defined propagation and growth/decay characteristics can be found in various ocean basins. Analyses in this and the next section are based on NCEP–NCAR reanalyses from June to September for the period of 1979–2003, unless indicated otherwise. An overview of the behavior of disturbances in the western Pacific and India/Bay of Bengal regions is given in Fig. 1. It shows the phase propagation vectors and growth rates of the 8-day high-pass-filtered vorticity at 850 hPa during the June to September season.[1] Information of the temporal coherence and teleconnectivity associated with the synoptic-scale eddies are also incorporated in Fig. 1. These statistics are computed following the methodology outlined by LL90 (see also LL90 for the interpretation of these quantities). Arrows being shown are located where the teleconnectivity exceeds the value of 0.35 and the temporal coherence is larger than 0.6. By choosing locations with high values of these two quantities, the arrows in Fig. 1 represent the propagation of disturbances with strong coherence and wavelike behavior.

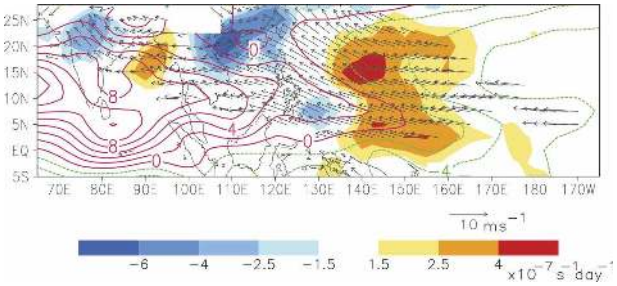

FIG. 1. Phase propagation vectors (arrows; see scale at lower right) and growth rates (shading; see scale bar) of the 8-day high-pass-filtered 850-hPa vorticity for the June–September period. Arrows are shown for locations where the temporal coherence of vorticity signals exceeds the value of 0.6 and teleconnectivity is greater than 0.35. The mean zonal wind (red contours for positive values and zero, green for negative values; interval: 2 m s^{-1}) at 850 hPa for the same period is also shown.

It can be seen that the synoptic-scale waves propagate westward or northwestward. Two major regions with an east–west-oriented growth-and-decay pattern can be found: one over the western Pacific with a broad spatial scale, and the other extending from the Bay of Bengal to northern India. The phase speed of the waves is about 5 m s^{-1} near the Philippines, and is faster in more eastward locations over the Pacific. The strongest growth of disturbances is located in the western Pacific at ~140°E. There is a portion of the Pacific storm tracks with strong growth rates that lies quite close to the equator. This could be related to mixed Rossby–gravity (MRG) wave activity in that region during the northern summer (Dickinson and Molinari 2002; Straub and Kiladis 2003).

This paper focuses on the synoptic-scale activity over the off-equatorial part of the western Pacific storm tracks where disturbances are initiated and begin to grow. In particular, the circulation structure and dispersion characteristics of eddies east of ~135°E will be examined. This is the region where strong growth rates are found and it is located on the southwestern rim of the Pacific subtropical high with mean easterlies in the low levels. This domain is also in the vicinity of the confluent zone of the western Pacific monsoon flow, where the zonal wind decelerates and changes sign far-

[1] Frequency spectra of the vorticity over many western Pacific locations show a peak at about 7–8 days (see also LL90). Results presented in Fig. 1 are not too sensitive to the choice of the cutoff frequency for time filtering.

ther west.[2] The confluent nature of the background flow is likely to be conducive to the growth of short Rossby waves due to the accumulation of wave activity and perhaps with the help of nonlinear processes (SB99; Kuo et al. 2001).

To obtain the dominant pattern of variability on synoptic time scales, the complex empirical orthogonal functions (EOFs) of the 8-day high-pass-filtered vorticity at 850 hPa are computed. The region of analysis is 10°–30°N, 140°E–160°W, and the first EOF explains about 10% of the domain-integrated variance. Figure 2 shows the regression coefficients of the 850-hPa vorticity upon the real part of the leading principal component (PC) time series at different time lags. By construction, the real part of the first EOF is the same as the regression map on day 0 within the aforementioned analysis domain (see Fig. 2b). The imaginary part of the EOF (not shown) is in quadrature in space with the real part. For the rest of the study, anomalies of meteorological fields related to this EOF are derived from regression based upon the real part of the leading PC.

Vorticity disturbances associated with this EOF are organized in the form of an east–west-oriented wave train. Anomalies exhibit a prominent northeast–southwest horizontal tilt, consistent with previous studies (see, e.g., LL90). Overall the wavelength ranges from 2000 to 3000 km. Based on the pattern on day 0 (Fig. 2b) and comparing the anomalies to the east and to the west of 150°E, a decrease of wavelength in the westward direction can be discerned. This is in accordance with the results of SB99, who demonstrated that there is a decrease of wavelength of Rossby wave packets as they enter a confluence region based on ray tracing. Disturbances are seen to propagate to the west, and the speed is about 6.5 m s^{-1} at 150°E. During the course of the evolution of the wave pattern, anomalies east of 135°E exhibit growth of their amplitude as they propagate. Those located west of 135°E on day −1 (Fig. 2a) eventually decay as they approach the east Asian coast (see Fig. 2c). Overall, the above-mentioned propagation and growth/decay characteristics are consistent with the results shown in Fig. 1. To ensure that these circulation patterns are robust and not artifacts due to time filtering, we have also computed composite maps based on unfiltered daily data of the vorticity field with its 9-day running mean removed. The method of compositing is similar to that used by LL90. The resulting spatial patterns as well as their temporal evolution (figures not shown) are very similar to those depicted in Fig. 2.

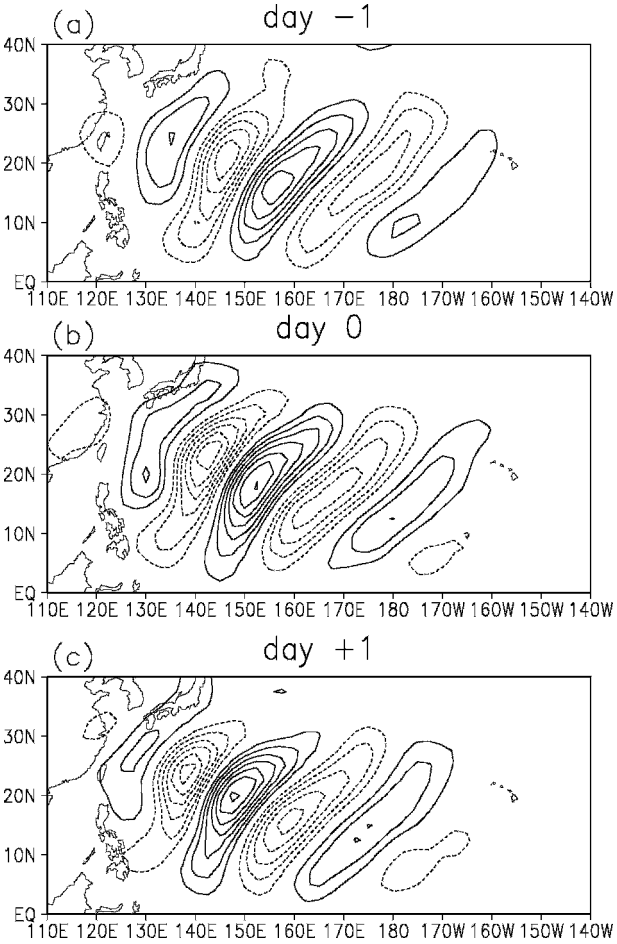

FIG. 2. Lag regression coefficients of 850-hPa vorticity upon the real part of the PC of the first complex EOF of vorticity at the same level, for the lag of (a) −1 day, (b) 0 day, and (c) +1 day. Contour interval: 0.5×10^{-6} s^{-1}. Dotted contours denote negative values. Zero contours are omitted.

Although most pronounced in the low levels, summertime synoptic-scale activity also has a significant impact on the upper-level circulation. Values of the regression of the winds and the correlation of the geopotential height at 200 and 850 hPa are given in Fig. 3, from day −1 to day +1. A wave train pattern can be clearly seen at both pressure levels. It is noticed that the geopotential field captures wave patterns that have centers of action aligned along the latitude of 20°N. The reduction of the zonal wavelength in the westward direction is also apparent at 850 hPa (see Fig. 3a). New circulation anomalies are being formed over the eastern part of the ocean as time progresses. It is noteworthy that over the central to eastern Pacific, upper-level circulation features tend to be more coherent than their

[2] The strongest deceleration of the mean easterlies can be found from the east of the Philippines to ~10°–20°N, 160°E.

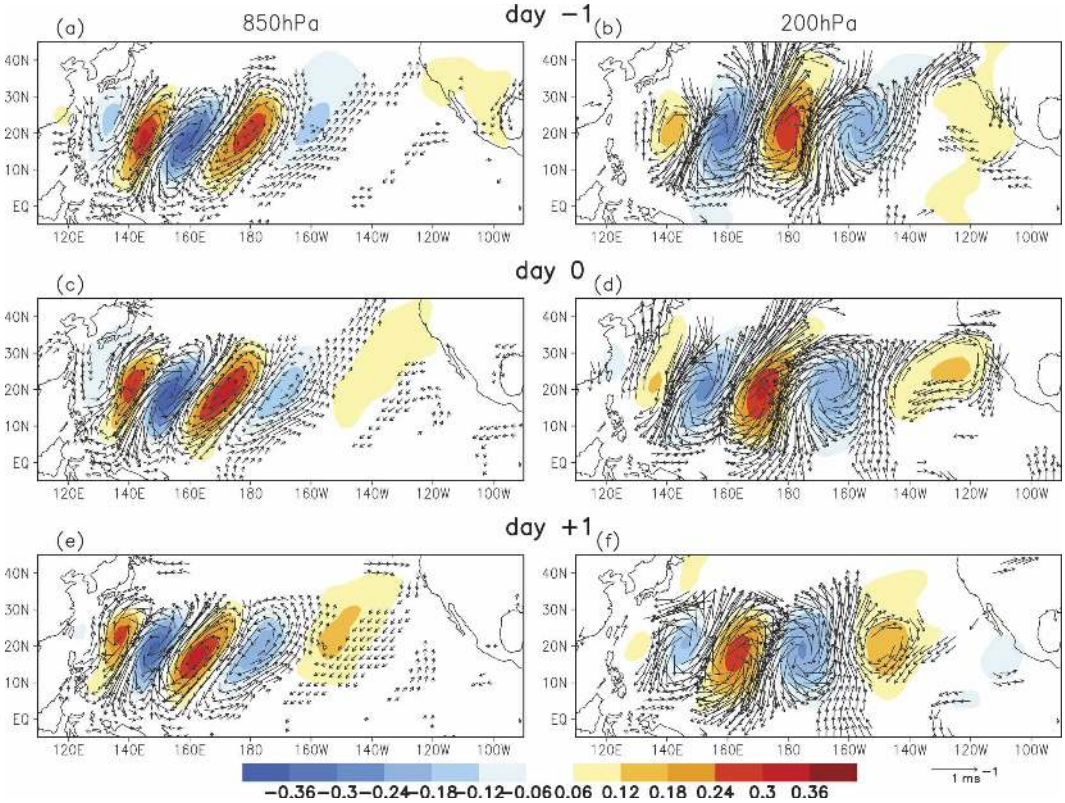

FIG. 3. Lag regression coefficients of the winds (arrows; see scale at lower right) and lag correlation of the geopotential height (shading; see scale bar at bottom) upon the real part of the leading PC of 850-hPa vorticity, for the lag of (a), (b) −1 day, (c), (d) 0 day, and (e), (f) +1 day, and for the (a), (c), (e) 850- and (b), (d), (f) 200-hPa levels. All wind and height field signals shown in this figure exceed the 95% significance level.

low-level counterparts at the same time lag. For instance, on day −1 an anticyclone at 200 hPa appeared near 120°W and the cyclone slightly east of 160°W was well formed. On the other hand, the circulation at the low level near the aforementioned locations was either poorly organized or less coherent in comparison (as evidenced by the smaller values of correlation coefficients). On day 0, the upper-level anticyclone in the eastern Pacific has developed, whereas the corresponding low-level circulation is just recognizable. The evolution of eddies portrayed here suggests that anomalies are first formed at the upper troposphere over the central to eastern Pacific, followed by downward development. In the next section, it will be shown that the group velocity of disturbances in this region is directed downward, supporting this interpretation.

4. Three-dimensional distribution of wave activity

a. Dispersion characteristics in low levels

To examine the dispersion characteristics of synoptic-scale disturbances, their associated wave-activity flux is computed. Results of Takaya and Nakamura (2001) are extended for a basic state with either positive or negative mean zonal wind (see appendix). The wave-activity vector can be shown to be parallel to the group velocity of Rossby waves in the plane wave limit. The calculation of this activity flux does not depend on any spatial or time averaging, making it ideal for depicting the three-dimensional pattern of wave activity at any particular instance. Furthermore, the wave-activity flux **W** and a pseudomomentum term M is related according to the equation

$$\partial_t M = -\nabla \cdot \mathbf{W} + S, \tag{1}$$

where S represents the forcing due to diabatic and frictional processes. Expressions for **W** and M can be found in the appendix. Here M is related to the eddy energy and enstrophy, and can be treated as a measure of the amplitude of disturbances. The above equation implies that convergence of wave activity or the forcing S can lead to the local growth of M, which can be interpreted as the amplification of waves in a phase-averaged sense.

Figure 4 gives the pseudomomentum M at 20°N (upper panel), the wave-activity flux (arrows in lower panel), and its divergence (shading in lower panel) at 850 hPa associated with the synoptic-scale disturbances, and regression of the height field (contours in lower panel) at the same vertical level on day 0. The pseudomomentum term and the activity flux are computed based on the geopotential height perturbations being shown.[3] The profile of M is reasonably consistent with the spatial modulation of the amplitude of the height field pattern. The most prominent feature of the flux pattern is that wave activity is almost everywhere directed to the west, basically following the mean wind. Li et al. (2003) also gave evidence that the wave energy of synoptic-scale disturbances moves to the west at ~160°E. There is also southward dispersion due to the northeast–southwest tilt of eddies. The westward-pointing wave activity or group velocity ($\mathbf{c}_g$) pattern can be understood from the Rossby wave dispersion relation. Assuming that these waves are barotropic Rossby waves and for small l/k, where $k(l)$ is the zonal (meridional) wavenumber, the zonal component of $\mathbf{c}_g$ is approximately given by $c_{gx} = U + \beta/k^2$. Here U is the mean zonal wind and β is the meridional gradient of the Coriolis parameter. For negative c_{gx}, the magnitude of the easterly mean wind should be larger than β/k^2 (such that the group velocity and the mean flow are in the same direction due to Doppler shifting). This condition is satisfied at locations east of ~135°E where the synoptic-scale disturbances are active. This is true for instance at 20°N, 150°E where $U \simeq 4$ m s^{-1} and the wavelength is about 2500 to 3000 km.

Convergence of wave activity[4] is found within the region of about 135°–160°E. Such convergence would lead to the amplification of waves, and its pattern is also consistent with the region of positive growth shown in Fig. 1. It is noteworthy that we have demonstrated explicitly the accumulation of wave activity within a wave packet. One can also estimate an e-folding time τ (or amplification rate τ^{-1}) from the activity flux convergence, following SB99. Taking the average over 15°–25°N, 135°–160°E for the quantities $-\nabla_H \cdot \mathbf{W}$ and M and dividing the former area average by the latter, the estimated value of τ^{-1} is about 1.62×10^{-6} s^{-1} (0.14 day^{-1}). Similarly, another e-folding time can also be estimated by dividing the growth rates given in Fig. 1 by the root-mean-squares of the high-pass-filtered vorticity. This gives a value of τ^{-1} for the abovementioned domain of about 4.28×10^{-7} s^{-1} (0.037 day^{-1}). The weaker amplification in the latter case is probably because values in Fig. 1 are statistical estimates. On the other hand, the activity flux convergence seen in Fig. 4 is relevant to a single wave train pattern. Nevertheless, these results support the idea that the accumulation of wave activity could be important for the growth of synoptic-scale activity in the region, as demonstrated by SB99 in a slightly different manner. It should be mentioned that wave activity accumulation and diabatic forcing are not mutually exclusive mechanisms of wave amplification. An estimate of the importance of diabatic processes will be given in section 6.

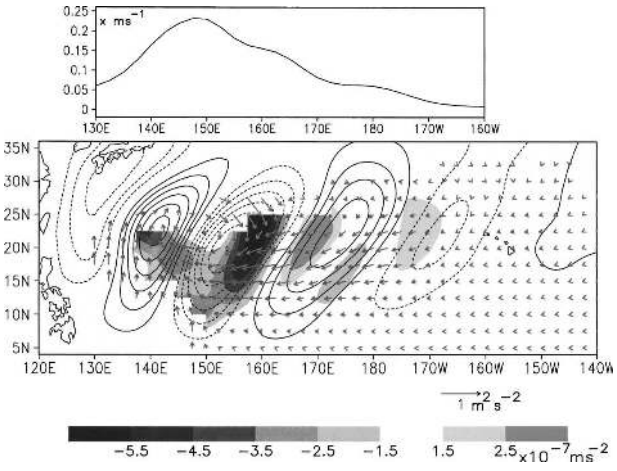

FIG. 4. Values of the (top) pseudomomentum term M at 20°N, and (bottom) wave-activity flux $\mathbf{W}$ (arrows; see scale at lower right) and its divergence (shading; see scale bar at bottom) at 850 hPa. Computation of $\mathbf{W}$ is based on the regression of the geopotential height upon the real part of the leading PC of 850-hPa vorticity on day 0. The geopotential pattern is also shown in the bottom panel (contours; interval: 0.5 m). Dotted contours denote negative values and zero contours are omitted.

In the plane wave limit the wave activity vector is given by $\mathbf{W} = M\mathbf{c}_g$. Thus the convergence of wave activity can be written as the sum of two terms, namely, that $-\nabla_H \cdot (M\mathbf{c}_g) = -\mathbf{c}_g \cdot \nabla_H M - M\nabla_H \cdot \mathbf{c}_g$. Again taking the average over the region of 15–25°N, 135°–160°E, it is found that the "advection term" $-\mathbf{c}_g \cdot \nabla_H M = -0.89 \times 10^{-2}$ m s^{-1} day^{-1}. This term is negative mainly because the group velocity is stronger on the eastern side of the wave packet where its amplitude is decreasing in the positive zonal direction (see upper panel of Fig. 4). There $\mathbf{c}_g$ is pointing up the gradient of M, making the advection term negative. The area-averaged value of the "convergence term" $-M\nabla_H \cdot \mathbf{c}_g$ is

[3] The wave-activity flux formulism is based on quasigeostrophy; the height field is thus proportional to the streamfunction, which is used for calculating the activity flux; see appendix.

[4] Here we approximate the three-dimensional divergence of wave activity with the horizontal divergence $\nabla_H \cdot \mathbf{W}$. It appears that in the low levels there is also convergence of activity in the vertical direction (see Fig. 9a). Its contribution to the three-dimensional convergence of $\mathbf{W}$ is about 20% at 775 hPa.

3.39×10^{-2} m s^{-1} day^{-1}. Further writing the group velocity as $\mathbf{c}_g = \mathbf{U} + \mathbf{c}_{gi}$, where $\mathbf{c}_{gi}$ is the intrinsic group velocity, and the convergence term equals to the sum of $-M\nabla_H \cdot \mathbf{U}$ and $-M\nabla_H \cdot \mathbf{c}_{gi}$, which have the value of 1.16×10^{-2} m s^{-1} day^{-1} and 2.23×10^{-2} m s^{-1} day^{-1}, respectively. Thus, the intrinsic group velocity $\mathbf{c}_{gi}$ contributes significantly to the accumulation of wave activity and is even more important than the mean flow convergence according to our estimates. This result is different from that of SB99, whose wave activity is dominated by the mean flow component over the western Pacific. A simple scale analysis suggests that their result is probably more relevant to disturbances with smaller spatial scales. In addition, their activity flux is computed based on the covariance statistics of all eddies (i.e., u' and $v'$are taken from the daily data of the winds). On the other hand, our analysis is built on the circulation associated with the leading EOF of the vorticity.

Since $\mathbf{c}_{gi}$ is determined by k and l, it is of interest to examine the spatial variation of these wavenumbers. Their values can be estimated using the relations $k^2 = \overline{v'^2}/\overline{\psi'^2}$ and $l^2 = \overline{u'^2}/\overline{\psi'^2}$. The terms $\overline{u'^2}$, $\overline{v'^2}$, and $\overline{\psi'^2}$ are the covariance of the u wind, v wind, and the streamfunction, respectively. Lag regression of the winds and streamfunction upon the leading PC of the 850-hPa vorticity are used as values for u', v', and ψ'. Covariance terms are then computed by summing up the products of regression coefficients from day -4 to day 4.

The estimated values of k^2 and l^2 at the latitude of 20°N are shown in Fig. 5a. It can be seen that k^2 increases from east to west. This is consistent with the height field pattern shown in Fig. 4 (see lower panel), which shows the decrease of the zonal wavelength in the westward direction. The quantity $k^2 - l^2$ also shows an increase in the negative zonal variation, with a larger magnitude. This is due to a decrease of l^2 to the west. Combining with the fact that k is increasing, it implies that, toward the west, eddies tend to be less tilted and their major axes point more to the meridional direction. Figure 5b shows the values of the term $\beta\,(k^2 - l^2)/(k^2 + l^2)^2$, which is the estimated zonal component of the intrinsic group velocity of Rossby waves. It decreases in the positive zonal direction in the region of ~130°–160°E, implying convergence of c_{gx}. As expected, this region is consistent with the convergence of activity flux shown in Fig. 4. Based on ray tracing, SB99 demonstrated that a Rossby wave packet would experience contraction of wavelength as its moves westward ($c_{gx} < 0$) in a confluent region ($\partial_x U < 0$) of mean easterlies. In other words, the local zonal wavenumber should increase to the west. Our finding is consistent with SB99's theoretical prediction, and such scale contraction leads to the convergence of the group velocity (hence wave activity).

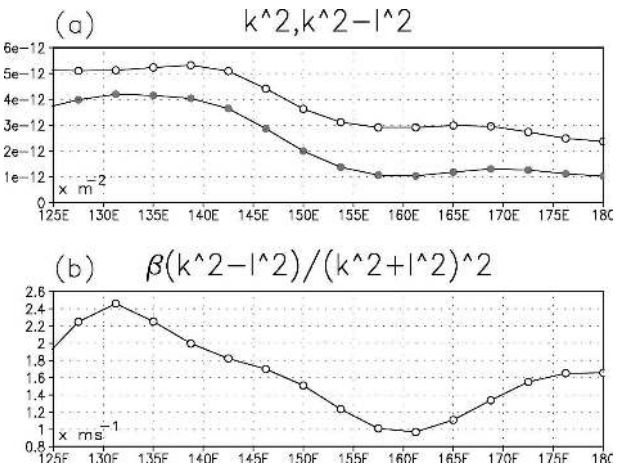

FIG. 5. (a) Values of the square of the zonal wavenumber k^2 (open circle) and the difference between the square of the zonal wavenumber and the square of the meridional wavenumber $k^2 - l^2$ (filled circle) at 20°N, based on the circulation pattern associated with the leading EOF of the 850-hPa vorticity. See text for details. (b) Values of $\beta\,(k^2 - l^2)/(k^2 + l^2)^2$ at 20°N.

In summary, we have demonstrated that there is accumulation of wave activity in the low levels associated with a wave packet of synoptic-scale disturbances over the western Pacific, and this occurs where the growth rate is strong. The accumulation of activity is mainly due to the convergence of group velocity of the waves. Contribution from the convergence of the intrinsic group velocity is about twice that due to the mean convergence. The former component is related to the spatial change of the zonal scale and the horizontal tilt of the waves, which can be attributed to the properties of the mean flow.

b. Vertical structure of circulation and wave activity

As shown previously, tropical synoptic-scale waves also have an impact on the upper-level circulation. Figures 6a and 6b show the vertical cross section of the regression coefficients of the vorticity and temperature from day -1 to day 0. The anomalous fields are averaged over the 15°–25°N latitude band. East of 150°E, the largest amplitude of vorticity perturbations is found at the 200-hPa level. To the west vortices are more confined to the middle to lower troposphere, and they are tilted westward in the vertical, similar to the results of LL90 (see their Fig. 16a). This vertical tilting structure is likely to be controlled by the vertical shear of the mean zonal wind (Holton 1971). Consistent with this idea, within the 15°–25°N band at about 150°E the difference between U at 200 and 850 hPa changes sign (see Fig. 8a with the mean zonal wind as contours).

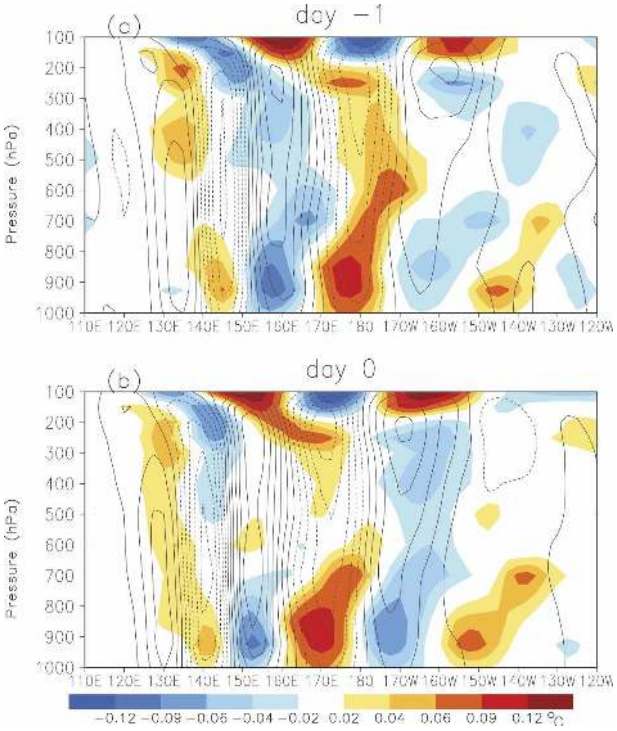

FIG. 6. Vertical cross sections of the regression of vorticity (contours, with dotted lines denoting negative values; interval: $0.5 \times 10^{-6}\ s^{-1}$) and temperature (shading; see scale bar at bottom) upon the real part of the leading PC of 850-hPa vorticity for the lag of (a) −1 day and (b) 0 day. Values of regression coefficients are averaged over the latitude band of 15°–25°N.

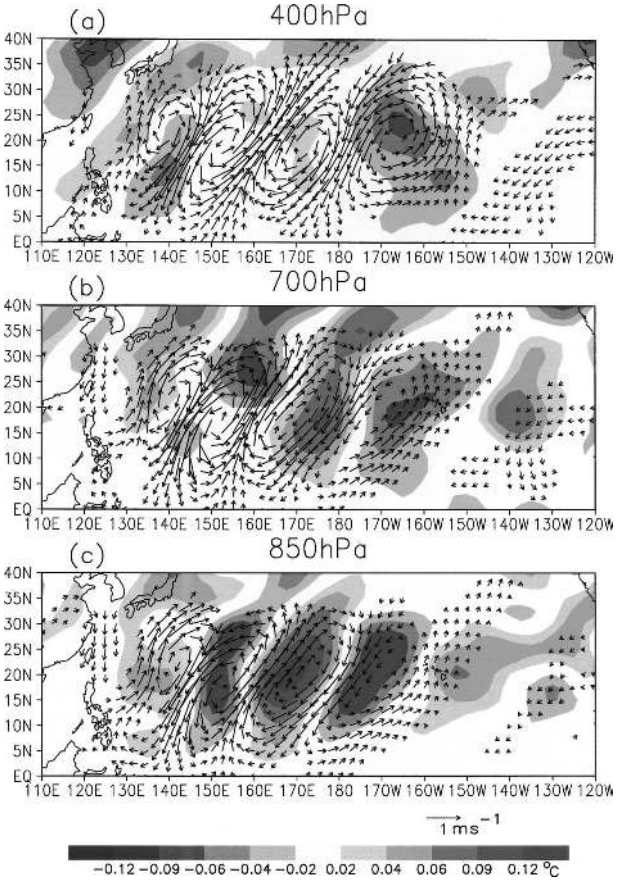

FIG. 7. Regression values of the winds (arrows; see scale at lower right) and temperature (shading; see scale bar at bottom) upon the real part of the leading PC of the 850-hPa vorticity on day 0, for the levels of (a) 400, (b) 700, and (c) 850 hPa. All wind regression values exceed the 95% significance level.

On day −1 (Fig. 6a), there is a strong positive vorticity anomaly at the upper level located at 160°W. It propagates to the west while extending downward (see Fig. 6b). At 850 hPa and below, there are cold (warm) temperature perturbations (T') collocated with positive (negative) vorticity signals (e.g., negative T' at 150°E and 170°W in the low levels; see Fig. 6b). The low-level "cold core" is a well-known signature of tropical synoptic-scale disturbances (LL90; Serra and Houze 2002). In the middle to lower troposphere (between 400 and 700 hPa) over the central to eastern Pacific, temperature anomalies are displaced to the east of the centers of vortices for about ⅛ to ¼ of a wavelength. This structure is especially obvious east of 160°E in the composite map for day −1 (Fig. 6a). There is also a corresponding phase relationship between the streamfunction (not shown) and temperature, namely, that cold (warm) anomalies are located east of negative (positive) streamfunction anomalies in the midlevels. This suggests that anomalies of the v-wind perturbations (v') are collocated with temperature anomalies of the opposite sign, that is, $v'T'$ is negative. Similar negative correlation between temperature and v wind near the central Pacific has been noticed in a number of studies concerning summertime synoptic-scale activity (e.g., Nitta 1970). Negative $v'T'$ has the important implication that the wave activity or group velocity is directed downward in this region, as will be shown later.

To ascertain the phase relationship between the wind and temperature, their regression coefficients on day 0 at the levels of 400, 700, and 850 hPa are plotted in Fig. 7. At 700 hPa (middle panel), southerly wind is clearly collocated with cold anomalies, and northerlies with warm anomalies. This happens over a broad region east of 150°E. At the 400-hPa level (top panel), there is still a region near 160°W with negative $v'T'$.[5] At 850 hPa (lower panel) and below (not shown) temperature and the v wind is positively correlated over the whole basin,

[5] Note that from 400 to 700 hPa and north of 10°–15°N, the mean temperature decreases poleward within 130°E–130°W.

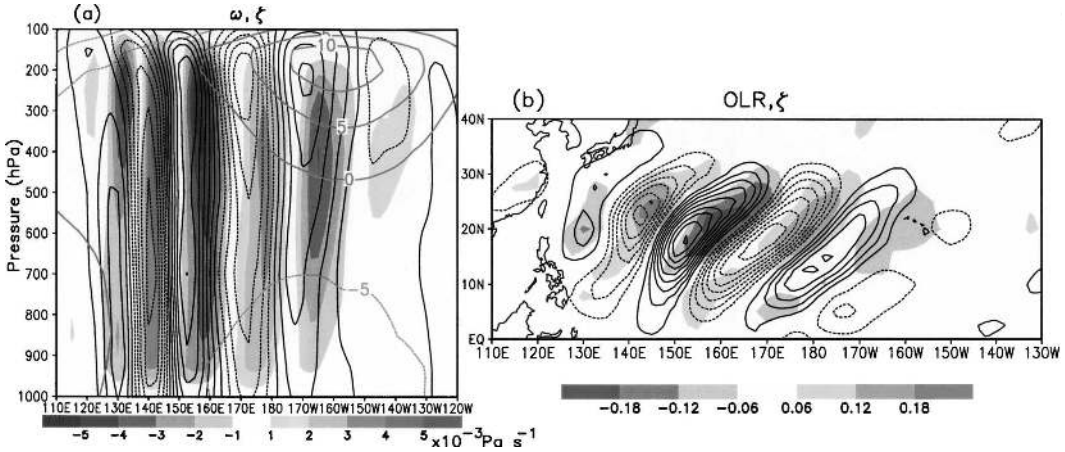

FIG. 8. (a) As in Fig. 6b, except that shading denotes the regression coefficient of the pressure velocity (see scale bar at bottom). Values of the June–September mean zonal wind averaged over 15°–25°N are also shown (thick contours with labels; interval: 5 m s^{-1}). (b) Correlation coefficient of 850-hPa vorticity (contours; interval: 0.06) and OLR (shading; see scale bar at bottom) based upon the real part of the leading PC of 850-hPa vorticity for day 0. Zero contours are omitted and dotted lines denote negative values for the vorticity correlation.

implying upward wave activity. Inspection of composite maps at other time lags (not shown) reveals the same phase relationship, namely, that negative $v'T'$ is found in the middle troposphere over the central to eastern Pacific.

The vertical cross section of the pressure velocity (ω') on day 0 is shown in Fig. 8a. Toward the west, the pressure velocity acquires a deeper structure and becomes stronger in the upper levels. Over the central to eastern Pacific, upward (downward) motion is located to the east of the positive (negative) vorticity anomalies for about 1/8 of a wavelength. West of ~150°E in the low levels, vertical motion in the middle to lower troposphere tends to coincide with the centers of strongest vorticity at the planetary boundary layer (PBL).

This longitudinal dependence of the phase relationship between ω' and vorticity is further supported by the OLR signals associated with the synoptic-scale disturbances. Negative OLR perturbations are indicative of enhanced convection and upward motion in the middle troposphere. Figure 8b gives the correlation coefficient between the OLR and the leading PC of the 850-hPa vorticity on day 0. The correlation between the 850-hPa vorticity and the PC time series is also shown. Daily data of OLR from NOAA for the period of 1979–2003 are used. There is a gradual change of the phase between the circulation and convection in the zonal direction. Enhanced convection is lagging the positive vorticity anomaly east of 150°E, while over the far western Pacific convective signals are almost in phase with vortices at 850 hPa. This is consistent with the relationship between the vertical motion and vorticity anomalies shown in Fig. 8a. The above analyses suggest that there are two different dynamical regimes along the western Pacific storm tracks. East of ~150°E the circulation appears to be governed by adiabatic dynamics; this point will be further elaborated below. To the west, rising motion is more related to convection. The latter is associated with the enhanced moisture at the PBL, as suggested by the strong specific humidity signals at 925 hPa over the far western Pacific (figure not shown). As a result, vertical motion is collocated with the low-level vorticity (and the associated Ekman pumping). It is also found that the magnitude of the regressed 500-hPa diabatic heating at 140°E is twice of that at ~170°W (figure not shown). It is likely that, in addition to the accumulation of wave activity, diabatic forcing is also important for the strong growth in the western portion of the storm tracks.

To gain insight on the relative importance of adiabatic motion in different portions of the wave train, consider the quasigeostrophic omega equation [see Eq. (6.29) of Holton 1992]:

$$\left(\nabla_H^2 + \frac{f_0^2}{\sigma}\partial_p^2\right)\omega' \approx \frac{f_0}{\sigma}\partial_p(U\partial_x\zeta' + \beta v') + \frac{R}{P\sigma}\nabla_H^2(\mathbf{u}\cdot\nabla T)'. \qquad (2)$$

The vorticity advection due to the mean flow on rhs is approximated by that due to U only. All symbols follow standard convections. The terms listed in (2) are computed from regression maps of various meteorological variables on day 0, and values of rhs are used to estimate lhs of (2). At 500–600 hPa and at the latitude of 20°N, the fractional error of the estimate is about 35%

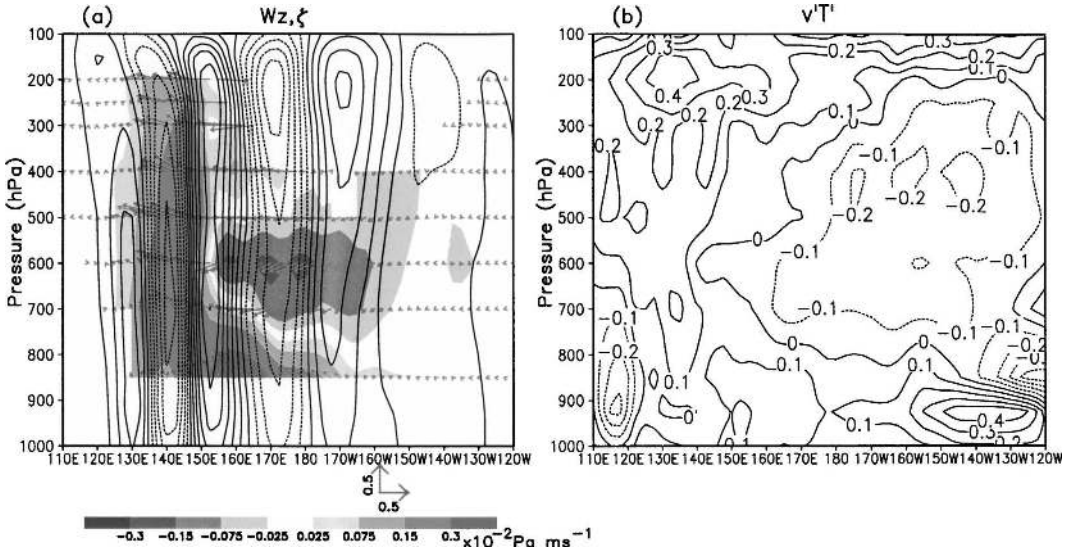

FIG. 9. (a) Vertical cross sections of the wave-activity vector (arrows; see lower right of left panel, with horizontal scale for 0.5 $m^2\ s^{-2}$ and vertical scale for 0.5×10^{-2} Pa $m\ s^{-1}$) and its vertical component (shading; see scale bar at bottom). Computation is based on the regression of geopotential at all levels upon the real part of the leading PC of 850-hPa vorticity on day 0, and final results are averaged over 15°–25°N. Also shown are the regression coefficients of vorticity as in Fig. 6b. (b) Values of the covariance between the 8-day high-pass-filtered v wind and temperature for the June–September period, averaged over 15°–25°N. Units: $m\ s^{-1}$ K.

east of 165°E, while averaged over 135°–165°E the error is about 70% (figures not shown). The result supports the idea that adiabatic dynamics is at least qualitatively valid in the eastern part of the synoptic-scale wave train. In contrast, convection is important in governing the vertical motion over the more western portion of the wave train.

We now use (2) to relate different components of the circulation associated with the synoptic-scale waves in the vicinity of the date line. Note that lhs of (2) is proportional to the vertical motion, that is, $[\nabla_H^2 + (f_0^2/\sigma)\partial_p^2]\omega' \propto -\omega'$. On day 0, there are strong signals of ω'at ~180° and 165°W in the middle troposphere of 400–500 hPa (see Fig. 8a). Since the temperature also has local maximum amplitudes at about the same locations (see Fig. 6b) and the term $\partial_p(\beta v') = \beta\partial_p(\partial_x\psi') \propto \partial_x T'$, the contribution of $\beta v'$ to rhs of (2) is small. To the east of the positive vortex centered at 170°W, the differential vorticity advection $\partial_p(U\partial_x\zeta')$ is positive due to the positive vertical shear of U there. This implies upward motion at ~160°–165°W, consistent with Fig. 8a. The temperature advection, that is, the last term in rhs of (2), is primarily proportional to $-v'\partial y\overline{T}$, which is also positive to the east of the vortex, implying even stronger upward vertical motion. Analogous arguments hold for locations east of the negative vorticity anomaly near 170°E (see again Fig. 8a); it can be readily determined that there is downward motion at about the date line.

Next, we present the vertical distribution of wave activity associated with the synoptic-scale disturbances. Figure 9a shows the cross section of the activity vector (arrows), its vertical component from 850 to 150 hPa (shading), and the corresponding vorticity perturbations (contours) on day 0. Computation of the activity flux is based on the regression of the geopotential height at each vertical level, and final results are averaged over the latitudinal band of 15°–25°N. There is a region from 150°E to 160°W, 400 to 700 hPa in which downward injection of wave activity can be found. In other words, there is incoming Rossby wave activity from the upper troposphere over the central Pacific region at about the entrance of the storm tracks. The downward-directed activity flux is due to the negative $v'T'$ in the abovementioned region (see Fig. 7). Below 700 hPa, and also west of 150°E at all vertical levels, wave activity is pointing upward.

Figure 9b shows the covariance between the v wind and temperature, averaged over the same band of 15°–25°N. Daily wind and temperature fields are 8-day high-pass filtered, and data for June to September are used to compute the statistics. Over the central to eastern Pacific there is a broad region with negative covariance between 300 and 700 hPa, which corresponds well with the locations where wave activity is directed downward (see Fig. 9a). This result supports our vertical wave activity distribution. Note that the covariance statistics encompass all eddy activity, whereas the activity

flux given in Fig. 9a is based on the circulation pattern associated with the synoptic-scale waves at one instance. The covariance pattern also suggests that downward energy dispersion is a robust feature at the entrance of the storm tracks near and to the east of the date line. More importantly, our analyses suggest that downward-directed wave activity may serve to initiate synoptic-scale disturbances, which subsequently propagate to the western Pacific and grow.

c. Activity source from upper levels

One fundamental question concerning the synoptic-scale variability over the western Pacific is the origin of the disturbances. Possible sources of wave activity include in situ ones such as mature tropical cyclones, and those related to easterly waves or TIWs in the eastern Pacific (see the introduction). Another possibility is forcing from the extratropics. Analyses in the previous subsection suggest that wave activity may originate from the upper troposphere. To make further connection with the upper-level activity, we have computed the **E** vector at 200 hPa given by $\mathbf{E} = [(\overline{v'^2} - \overline{u'^2})/2, -\overline{u'v'}]$ (Trenberth 1986). The covariance terms are calculated based on regression coefficients of u and v upon the leading PC time series of the 850-hPa vorticity, and their products are summed over the lags of -8 days to $+8$ days. These **E** vectors therefore represent upper-level activity closely associated with the tropical synoptic-scale disturbances. Figure 10 shows the results of this calculation. The strongest **E** vectors are located in the tropical regions. Energy dispersion is predominately directed to the south, consistent with the horizontal tilt of eddies (see right panels of Fig. 3). It is worth noticing that a clear pattern of **E** vectors also appears in the midlatitudes. In fact, there is evidence that the midlatitude pattern captured in Fig. 10 is due to baroclinic waves. For instance the diffluent pattern at about 40°N, 150°E and the eastward pointing vectors at the jet core are typical features of the **E** vectors associated with baroclinic eddies (see, e.g., Hoskins et al. 1983). There is a stream of strong southward pointing vectors near the date line that extends almost continuously from the Pacific jet to the Tropics. Regression maps of the 200-hPa circulation (figures not shown) also show hints of a wave train that originated near the Asian coast at about 40°–50°N and reached the tropical central to eastern Pacific. Eddies within this wave train have a prominent northeast–southwest tilt, giving rise to the dominant southward dispersion in Fig. 10.

The **E**-vector pattern strongly suggests that there is a linkage between tropical synoptic-scale disturbances and extratropical activity. According to linear theory, however, absorption of wave activity occurs near the critical line of $U \sim 5$–10 m s^{-1}. Wave activity from the extratropics indeed seems to be weaker within part of this critical region, say near 30°N, 150°W. However, there is also a penetration zone of southward wave activity into the Tropics near the date line (see Fig. 10). One possibility is that the summertime synoptic-scale disturbances might be related to PV intrusion into the Tropics or Rossby wave breaking. The latter phenomenon is also known to be active over the subtropical central Pacific at the tropopause level during boreal summer (Postel and Hitchman 1999). In the next section, a case study will be presented in which midlatitude upper-level disturbances are able to initiate tropical synoptic-scale activity.

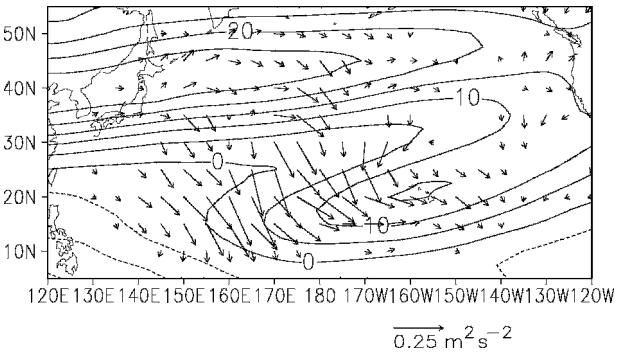

FIG. 10. **E** vectors (arrows for magnitude greater than 0.02 m^2 s^{-2}; see scale at lower right) at 200 hPa based on the circulation associated with the first EOF of the 850-hPa vorticity. See text for details. Also shown is the mean 200-hPa zonal wind (contours; interval: 5 m s^{-1}) during the June–September season.

5. A case study

For a case study of the initiation and growth of tropical disturbances over the western Pacific region, the synoptic situation for the period of 1 to 5 September 2001 is examined. Data in this section comprise the upper-air reanalyses from ERA-40 and QuikSCAT surface winds. Figures 11a and 11e show the day-to-day evolution of PV at the 350-K potential temperature surface during this period. The 31-day mean PV and zonal wind centered on 1 September at the same surface is also shown (Fig. 11f).

The most striking feature in the daily maps is the east–west-oriented strip of high PV at about 25°–30°N, east of the date line (see, e.g., Figs. 11a–c). The high PV values at about 165°W were associated with circulation anomalies that extended to the middle troposphere (see left panels of Fig. 12a). It will be shown below that the intrusion of high PV and its undulation was accompanied by the development of a synoptic-scale wave train in the Tropics. Inspection of PV maps a few days before

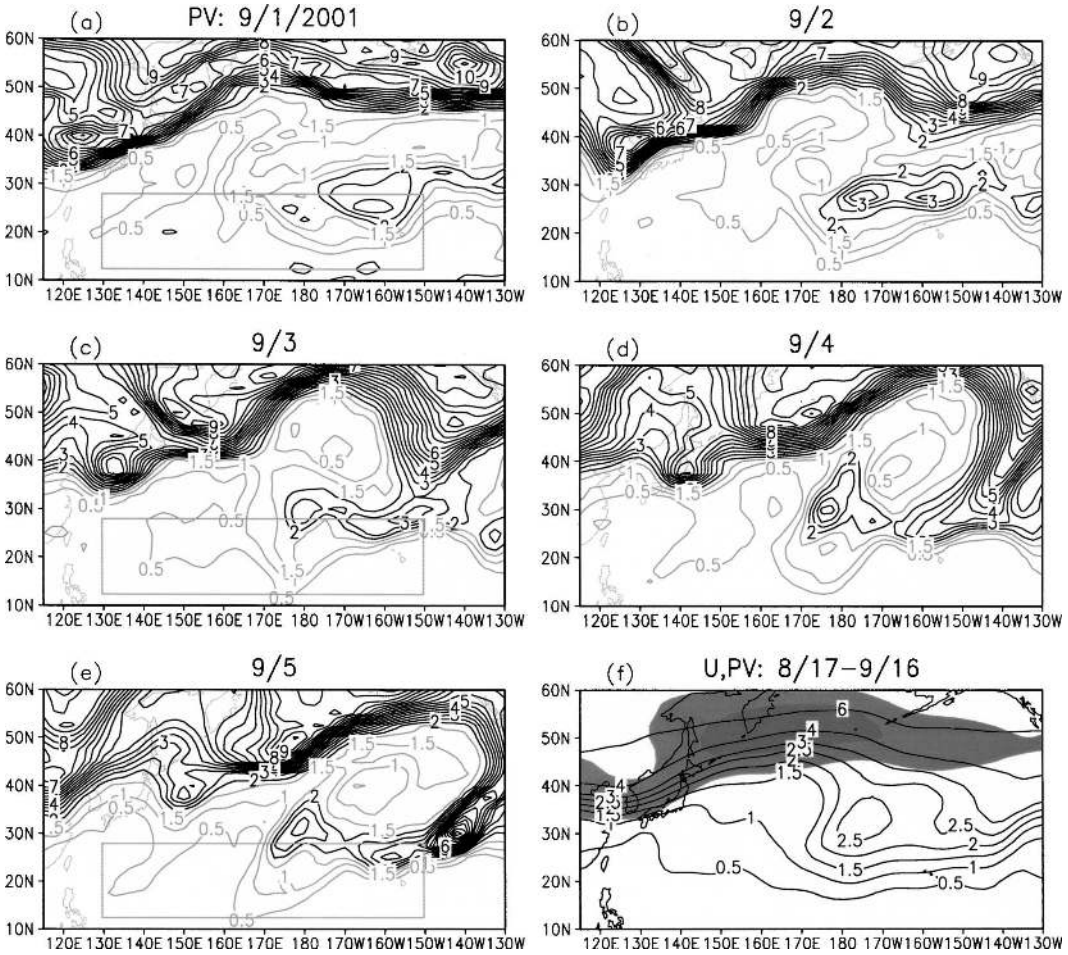

FIG. 11. PV at the 350-K potential temperature surface on the day of (a) 1, (b) 2, (c) 3, (d) 4, and (e) 5 Sep 2001 (contour interval: 0.5 PVU; 1 PVU = 10^{-6} K m^2 kg^{-1} s^{-1}). Dotted contours are used for 0.5, 1, and 1.5 PVU; regions with PV greater than 2 PVU are lightly shaded. (f) Values of the 31-day mean, centered on 1 Sep 2001, of the 350-K PV (contour; interval: 0.5 PVU) and zonal wind (light shading for values between 20 and 30 m s^{-1}; dark shading for those greater than 30 m s^{-1}). Boxes in (a), (c), and (e) mark out the tropical region where disturbances in the low levels were initiated (see upper panel of Figs. 12a–c).

(figures not shown) reveals that this high PV patch arose due to a wave-breaking event. On 29 August, an anticyclone centered at ~35°–40°N caused high PV air to its east to move southwestward. On 1 September part of the high PV patch became cut off from the extratropical circulation. The evolution just described is in accordance with the LC1 paradigm (Thorncroft et al. 1993; see also Postel and Hitchman 1999). A similar event occurred during the period of 3–5 September, resulting in high PV air at ~150°W reaching the tropical latitudes (see Figs. 11c–e). In fact, the rather spatially uniformed mean PV in the vicinity and to the south of the jet exit (as indicated by the 2.5-PVU contours in Fig. 11f) suggests that wave breaking was likely to occur. It is noteworthy that on 4 and 5 September there were many northeast–southwest-tilted features (Figs. 11d–e). Such tilting is consistent with the **E**-vector plot of Fig. 10.

Figures 12a–c show the anomalous PV at 350 K (upper left panel of each figure), vorticity and temperature anomalies averaged over the 15°–22.5°N band (vertical cross section, lower left panel), and wind and vorticity anomalies at the surface (right panel) on 1, 3, and 5 September, respectively. Anomalies of various fields are defined as the daily values with their 31-day mean centered on 1 September removed. On 1 September, the positive PV anomaly at ~160°W over Hawaii (upper left panel of Fig. 12a) was associated with enhanced vorticity reaching the middle troposphere and cold perturbations located to the east (see cross sections in middle panel). Farther west within the same latitudes, there were vorticity anomalies with rather deep vertical

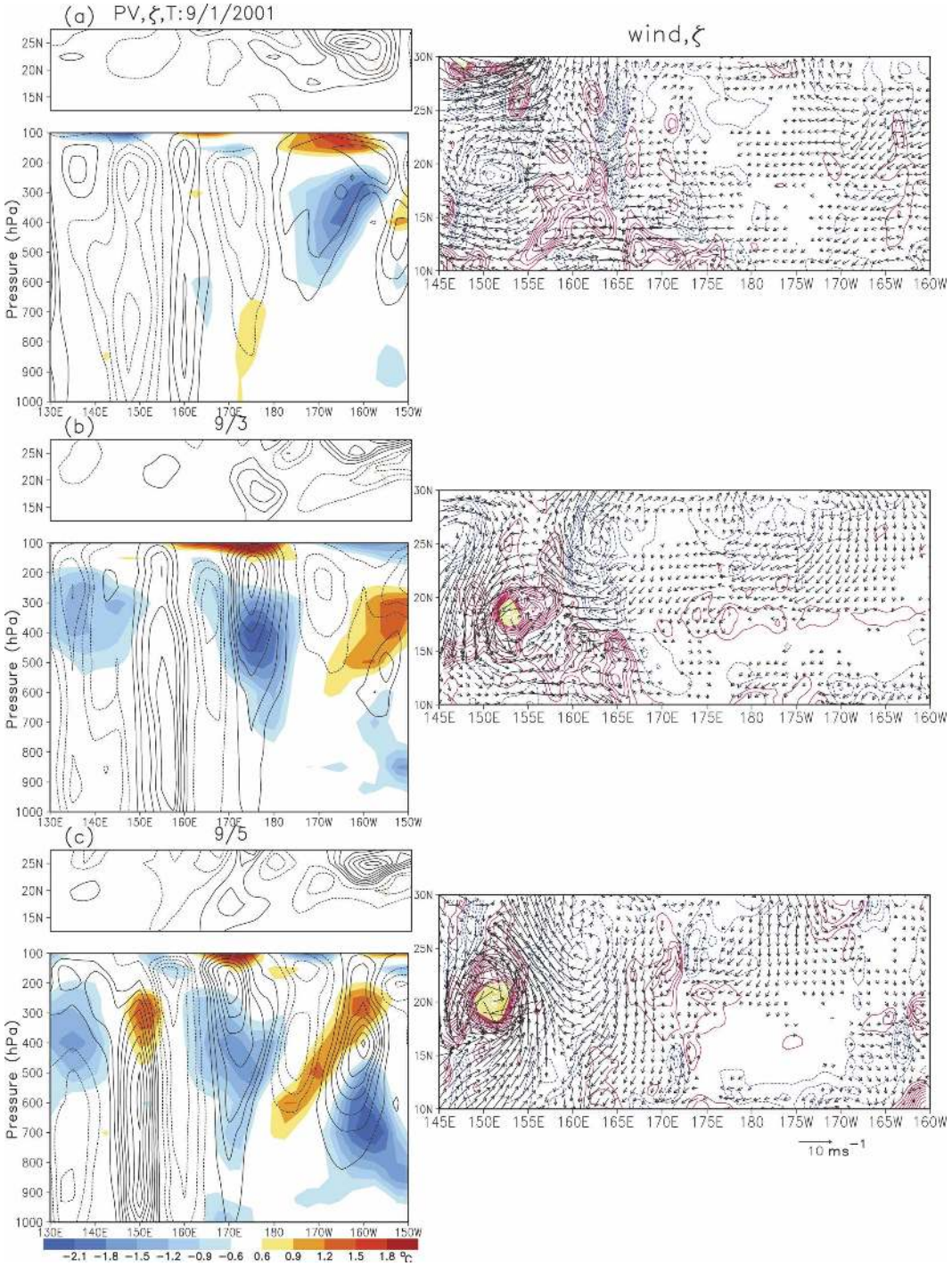

FIG. 12. (left top panels) PV anomalies at the 350-K surface (contours; interval: 0.25 PVU); (left bottom panels) 15°–22.5°N vertical cross sections of anomalous vorticity (contours; interval: 5×10^{-6} s^{-1}) and temperature [shading; see scale bar at lower left of (c)], and (right panels) QuikSCAT surface wind [arrows for speed greater than 1 m s^{-1}; see scale at lower right of (c)] and vorticity (with blue contours for negative values, interval: 5×10^{-6} s^{-1}; red for values between 0.5×10^{-5} s^{-1} and 5.5×10^{-5} s^{-1}, interval: 5×10^{-6} s^{-1}; yellow for values greater than 5.5×10^{-5} s^{-1}, interval: 10^{-5} s^{-1}), for the day of (a) 1, (b) 3, and (c) 5 Sep 2001. Zero contours are omitted and dotted lines denote negative values for the anomalous PV and vorticity. Anomalies of meteorological fields are defined as the departure from their corresponding 31-day means centered on 1 Sep 2001.

structures, for instance, the anticyclonic vortex located at 150°E and the cyclonic one at 160°E. They were accompanied with surface flow perturbations of the same circulation sense (right panel). However, the middle- to upper-level circulation systems east of 170°E had little discernable effects at the surface.

On 3 September (Fig. 12b), the two vortices originally located over the central Pacific had propagated westward and acquired a deep structure. Their corresponding circulation patterns at the surface can be found at ~165° and 175°E. A tropical storm was formed at 155°E within the positive vortex in the western part of the wave train (vortex with yellow contours in the right panel of Fig. 12b). In more eastern locations, another circulation system associated with the negative PV anomaly near the tropopause appeared over the central to eastern Pacific.

Two days later on 5 September the positive vortex originally found near the date line moved farther west to 170°E (Fig. 12c). Low-level cold perturbation was found near its center, typical of tropical synoptic-scale waves. There was also obvious growth of its associated vorticity signals at the surface. In the eastern part of the domain, upper-level disturbances became deeper, and new anomalies continued to appear. It is noteworthy that the evolution of the synoptic-scale disturbances portrayed here, and the phase relationship between different variables, resemble those presented in the previous section (see Fig. 6). It is also noticed that strong cold (warm) perturbations tended to be located to the east of positive (negative) vortices (see lower left panels of Figs. 12a–c) over the central to eastern Pacific. Examination of the circulation at 600 hPa (not shown) reveals that negative correlation between temperature and the v wind was particularly strong when the upper-level vortices were extending downward. This is the case for the positive vortex at 170°W (175°E) on 1 September (3 September), and also for the negative vortex at 170°W (175°W) on 3 September (5 September). In other words, there were robust signatures of downward-directed wave activity during the course of the evolution of the wave train. Overall, results of this case study strongly support the idea that upper-tropospheric wave activity can initiate disturbances with strong low-level signatures over the tropical western Pacific through downward Rossby wave dispersion.[6]

[6] Maps of OLR anomalies during this period are also examined (figures not shown). There were no discernable OLR signals east of the date line on 1 September. Thus it seems unlikely that the downward extension of the vortex centered at 170°W on that day was due to convection.

6. Discussions and conclusions

In this study, the initiation, growth, and three-dimensional dispersion of the summertime synoptic-scale disturbances in the western Pacific are examined. Over the region with strong growth of vorticity perturbations, the dominant mode of variability exhibits a wave train pattern with westward phase propagation. Wave-activity diagnostics reveal westward-directed group velocity associated with the wave packet. There is accumulation of wave activity in the low levels, which could lead to strong growth of the waves. Such accumulation can be attributed to two major components: one that results from the convergence of the intrinsic group velocity and one due to the mean flow convergence. The former component has the larger contribution to the activity accumulation and is related to the shortening of wavelength in the westward direction. The location of activity flux convergence is also consistent with where the strongest growth rates of synoptic-scale disturbances are found. These results support the idea that wave activity accumulation could be important for the growth of disturbances over the western Pacific, as proposed by SB99.

Over the central to eastern Pacific where disturbances begin to be manifested in the low levels, their corresponding upper-level circulation features tend to be better formed. There is prominent equatorward heat flux associated with the disturbances in the region and wave activity is directed downward from ~300–400 to 700 hPa. Further analysis shows that in the upper troposphere there is associated activity flux that penetrates from the extratropics into the tropical Pacific. These findings suggest that upper-level activity with extratropical origins can initiate summertime synoptic-scale disturbances. This hypothesis about the triggering of synoptic-scale waves is supported by a case study, in which low-level circulation anomalies were induced by the intrusion of strong upper-level PV into the Tropics. This is in accordance with the results of Heta (1991), who reported that synoptic-scale waves seemed to be accompanied with upper-level disturbances that originated over the tropical central Pacific. It should be emphasized that this initiation mechanism is most relevant to disturbances in the vicinity of the subtropical Pacific. Also, it does not rule out the possibility of MRG waves "seeding" (see SB99 and references therein) or random convection exciting the synoptic-scale disturbances.

Besides studying the dispersion characteristics of the tropical synoptic-scale waves within a quasigeostrophic framework, we also seek to understand the roles of diabatic processes. As inferred from the structure of the waves, and from analyses based on the omega equation,

TABLE 1. Wave activity budget averaged over days −1 to −3, for the region of 15°–20°N, 135°–160°E. Computation is based on regression coefficients of geopotential height upon the real part of the leading PC of 850-hPa vorticity. In parentheses are the ratios of the flux convergence and residue terms to the total tendency $\partial_t M$. Units: 10^{-2} m s^{-1} day^{-1}.

	400 hPa	500 hPa	600 hPa	700 hPa
$\partial_t M$	2.925	4.235	4.02	3.66
$-\nabla_H \cdot \mathbf{W}$	2.21 (76%)	1.94 (46%)	1.92 (48%)	1.745 (48%)
$\partial_p W_p$	0.035 (1%)	−0.19 (−4%)	0.27 (7%)	0.735 (20%)
Residue S	0.68 (23%)	2.48 (58%)	1.83 (45%)	1.18 (32%)

there are two dynamical regimes along the storm tracks. In the vicinity of the date line, adiabatic dynamics is qualitatively valid and is useful for understanding the three-dimensional circulation associated with the disturbances. Over the more western portion of the wave train where the vorticity and rising motion are in phase, diabatic heating is important in determining the circulation.

To assess the contribution of diabatic processes to the growth of synoptic-scale disturbances, the budget of wave activity is computed based on (1). Wave activity averaged over day −1 to day −3 and the corresponding tendency of M is used. The term S in (1) is calculated as a residue, and it provides an estimate of the diabatic forcing. Results are area averaged over the region of 15°–20°N, 135°–160°E and their values at various vertical levels are shown in Table 1. It can be seen that S is most important at 500 to 600 hPa and it contributes as much as about 60% to the tendency of M. Away from the middle troposphere at the levels of 400 and 700 hPa, diabatic effects are comparatively weaker and wave amplification is mainly attributed to the convergence of $\mathbf{W}$. The results indicate that wave activity accumulation is at least as important as the forcing due to diabatic processes (presumably condensational heating) for the growth of the synoptic-scale waves.

Our results reflect those of Kiladis (1998) concerning the ITCZ convective activity forced by Rossby waves from the extratropics. Equatorward and downward dispersion of waves are also found prior to the enhancement of convection, reminiscent of the three-dimensional dispersion in our study. In contrast to the results of Kiladis (1998), we could not find wave trains from the extratropics with centers of action that are clearly geographically fixed in our regression maps of the upper-level circulation (figures not shown). The submonthly time scales considered by Kiladis (1998) probably lead to teleconnection patterns that are more fixed in space. Moreover, PV intrusion or cutoffs could be intermittent and could occur at different locations, depending on the background flow. These factors would make a fixed wave train pattern unlikely to appear in our composite maps.

It is of interest that Rossby wave breaking is also active over the central to western Atlantic at the tropopause level during boreal summer (Postel and Hitchman 1999). However, maps of the v wind and temperature covariance do not show any strong equatorward heat flux that extends to the middle troposphere in that region, unlike the situation over the Pacific (figure not shown). Thus there seems to be no robust sign of downward wave activity over the tropical Atlantic during boreal summer.

Finally, in view of the initiation mechanism revealed in this study, western Pacific synoptic-scale activity could be linked to elements of the midlatitude circulation such as the structure of the Pacific jet. Our preliminary study suggests that changes of the jet on interannual time scale could be another important source of variability for the western Pacific region besides ENSO. Results of this research effort will be reported elsewhere.

Acknowledgments. We are grateful to Hisashi Nakamura for suggestions and encouragement and to Russell Elsberry, Hung-Chi Kuo, Gabriel Lau, Yolande Serra, Julia Slingo, and Bin Wang for discussions. Comments from George Kiladis and three anonymous reviewers helped to strengthen this paper. B. Fu prepared the QuikSCAT data. Tim Li is supported by the National Science Foundation under Grant ATM-01-19490, and by DOD/ONR Grants N000140310739 and N000140210532. The International Pacific Research Center is partially supported by Japan Agency for Marine-Earth Science and Technology.

APPENDIX

Wave-Activity Flux Formulation

Expressions for the phase-independent wave-activity flux of Takaya and Nakamura (2001), generalized for a basic state with either easterly or westerly mean wind, are given here. For an unforced quasigeostrophic flow, it can be readily shown that the mean PV gradient $\nabla_H Q$

is parallel to the mean flow $\mathbf{U}$, that is, $\mathbf{U} \cdot \nabla_H Q = 0$. Therefore the unit vector $\hat{\mathbf{U}}$ can be written as $\hat{\mathbf{U}} = \gamma \nabla_H Q / |\nabla_H Q| \times \hat{\mathbf{e}}_z$, where $\hat{\mathbf{e}}_z$ is the unit vector in the vertical direction. For γ equals to 1 (-1), the flow is said to be "pseudoeastward" ("pseudowestward") (Andrews 1984). The wave-activity vector $\mathbf{W}$ is given by

$$\mathbf{W} = \frac{\gamma}{2|\mathbf{U}|} \begin{pmatrix} U(\psi_x^2 - \psi\psi_{xx}) + V(\psi_x\psi_y - \psi\psi_{xy}) \\ U(\psi_x\psi_y - \psi\psi_{xy}) + V(\psi_y^2 - \psi\psi_{yy}) \\ \frac{f_0^2}{S_p}[U(\psi_x\psi_p - \psi\psi_{xp}) + V(\psi_y\psi_p - \psi\psi_{yp})] \end{pmatrix} + Cp\hat{\mathbf{U}}M.$$

In this expression, U and V denote the mean wind components, and ψ is the perturbation streamfunction, which is assumed to be proportional to the geopotential height in quasigeostrophic (QG) approximation; S_p is the static stability parameter and f_0 is the Coriolis parameter. Subscripts denote partial derivatives. The pseudomomentum term $M = \frac{1}{2}\{\frac{1}{2}[q^2/|\nabla_H Q|] + [(\gamma e)/(|\mathbf{U}| - C_p)]\}$, where q and e are the PV and energy of eddies, respectively, and C_p is the phase speed measured along the direction of the mean flow. In deriving the above expressions, we followed Takaya and Nakamura (2001) without assuming that γ equals one. Their derivations can be carried over by multiplying rhs of their Eqs. (14) and (22) with the factor γ.

The phase-independent wave activity formulation is applied to synoptic-scale disturbances within regions where U is negative, and therefore γ equals -1. Here C_p is estimated based on the phase propagation of the relativity vorticity at 850 hPa following LL90. The values of C_p are consistent with those predicted by the Rossby wave dispersion relation, given the local wavenumber, the mean PV gradient, and the wind speed.

REFERENCES

Andrews, D. G., 1984: On the existence of nonzonal flows satisfying sufficient conditions for stability. *Geophys. Astrophys. Fluid Dyn.,* **28,** 243–256.

Chang, C.-P., V. F. Morris, and J. M. Wallace, 1970: A statistical study of easterly waves in the western Pacific: July–December 1964. *J. Atmos. Sci.,* **27,** 195–201.

Dickinson, M., and J. Molinari, 2002: Mixed Rossby–gravity waves and western Pacific tropical cyclogenesis. Part I: Synoptic evolution. *J. Atmos. Sci.,* **59,** 2183–2196.

Heta, Y., 1991: The origin of tropical disturbances in the equatorial Pacific. *J. Meteor. Soc. Japan,* **69,** 337–351.

Holland, G. J., 1995: Scale interaction in the western Pacific monsoon. *Meteor. Atmos. Phys.,* **56,** 57–79.

Holton, J. R., 1971: A diagnostic model for equatorial wave disturbances: The role of vertical shear on the mean zonal wind. *J. Atmos. Sci.,* **28,** 55–64.

——, 1992: *An Introduction to Dynamic Meteorology.* Academic Press, 511 pp.

Hoskins, B. J., I. N. James, and G. H. White, 1983: The shape, propagation and mean-flow interaction of large-scale weather systems. *J. Atmos. Sci.,* **40,** 1595–1612.

Kalnay, E., and Coauthors, 1996: The NCEP/NCAR 40-Year Reanalysis Project. *Bull. Amer. Meteor. Soc.,* **77,** 437–471.

Kiladis, G. N., 1998: Observations of Rossby waves linked to convection over the eastern tropical Pacific. *J. Atmos. Sci.,* **55,** 321–339.

Kistler, R., and Coauthors, 2001: The NCEP–NCAR 50-year reanalysis: Monthly means CD-ROM and documentation. *Bull. Amer. Meteor. Soc.,* **82,** 247–267.

Kuo, H.-C., J.-H. Chen, R. T. Williams, and C.-P. Chang, 2001: Rossby waves in zonally opposing mean flow: Behavior in northwest Pacific summer monsoon. *J. Atmos. Sci.,* **58,** 1035–1050.

Lau, K.-H., and N.-C. Lau, 1990: Observed structure and propagation characteristics of tropical summertime synoptic scale disturbances. *Mon. Wea. Rev.,* **118,** 1888–1913.

——, and ——, 1992: The energetics and propagation dynamics of tropical summertime synoptic-scale disturbances. *Mon. Wea. Rev.,* **120,** 2523–2539.

Legeckis, R., 1977: Long waves in the eastern equatorial Pacific Ocean: A view from a geostationary satellite. *Science,* **197,** 1179–1181.

Li, T., B. Fu, X. Ge, B. Wang, and M. Peng, 2003: Satellite data analysis and numerical simulation of tropical cyclone formation. *Geophys. Res. Lett.,* **30,** 2122, doi:10.1029/2003GL018556.

Nitta, T., 1970: On the role of transient eddies in the tropical troposphere. *J. Meteor. Soc. Japan,* **48,** 348–359.

——, and Y. Takayabu, 1985: Global analysis of the lower tropospheric disturbances in the Tropics during the northern summer of the FGGE year. Part II: Regional characteristics of the disturbances. *Pure Appl. Geophys.,* **123,** 272–292.

Postel, G. A., and M. H. Hitchman, 1999: A climatology of Rossby wave breaking along the subtropical tropopause. *J. Atmos. Sci.,* **56,** 359–373.

Reed, R. J., and E. E. Recker, 1971: Structure and properties of synoptic-scale wave disturbances in the equatorial western Pacific. *J. Atmos. Sci.,* **28,** 1117–1133.

Riehl, H., 1945: Waves in the easterlies and the polar front in the tropics. Miscellaneous Rep. 17, Department of Meteorology, University of Chicago, 79 pp.

Serra, Y. L., and R. A. Houze Jr., 2002: Observations of variability on synoptic timescales in the east Pacific ITCZ. *J. Atmos. Sci.,* **59,** 1723–1743.

Sobel, A. H., and C. S. Bretherton, 1999: Development of synoptic-scale disturbances over the summertime tropical northwest Pacific. *J. Atmos. Sci.,* **56,** 3106–3127.

Straub, K. H., and G. N. Kiladis, 2003: Interactions between the boreal summer intraseasonal oscillation and higher-frequency tropical wave activity. *Mon. Wea. Rev.,* **131,** 945–960.

Takaya, K., and H. Nakamura, 2001: A formulation of a phase-

independent wave-activity flux for stationary and migratory quasigeostrophic eddies on a zonally varying basic flow. *J. Atmos. Sci.,* **58,** 608–627.

Thorncroft, C. D., B. J. Hoskins, and M. E. McIntyre, 1993: Two paradigms of baroclinic-wave life-cycle behaviour. *Quart. J. Roy. Meteor. Soc.,* **119,** 17–55.

Trenberth, K. E., 1986: An assessment of the impact of transient eddies on the zonal flow during a blocking episode using localized Eliassen–Palm flux diagnostics. *J. Atmos. Sci.,* **43,** 2070–2087.

Wallace, J. M., 1971: Spectral studies of tropospheric wave disturbances in the tropical western Pacific. *Rev. Geophys. Space Phys.,* **9,** 577–612.

——, and C.-P. Chang, 1969: Spectrum analysis of large-scale wave disturbances in the tropical lower troposphere. *J. Atmos. Sci.,* **26,** 1010–1025.